Electronic Supplementary Information

Lithium doped nickel oxide nanocrystals with a tuned electronic structure for oxygen evolution reaction

Ziyi Xiao,[a] Wei Zhou,[b] Ning Zhang,[a, c] * Chengan Liao,[a] Shicheng Huang, [a, f] Guoxin Chen,[d] Gen Chen,[a] Min Liu,[d] Xiaohe Liu,[a] and Renzhi Ma [e]

[a] School of Materials Science and Engineering, Central South University, Changsha 410083, Hunan , P. R. China
Email: nzhang@csu.edu.cn

[b] Department of Applied Physics, Tianjin Key Laboratory of Low Dimensional Materials Physics and Preparing Technology, School of Science, Tianjin University, Tianjin 300072, P. R. China

[c] Guangdong Provincial Key Laboratory of Technique and Equipment for Macromolecular Advanced Manufacturing, South China University of Technology, Guangzhou 510640, Guangdong, P. R. China

[d] School of Physical Science and Electronics Central South University, Changsha, Hunan 410083, P. R. China

[e] Ningbo Institute of Materials Technology & Engineering Chinese Academy of Sciences No. 1219 Zhongguan West Road Zhenhai District Ningbo, Zhejiang 315201, P. R. China

[e] International Center for Materials Nanoarchitectonics (MANA) National Institute for Materials Science (NIMS) 1-1 Namiki, Tsukuba, Ibaraki 305-0044, Japan

[f] Guangxi Crystal Union Photoelectric Materials Co. Ltd., No. 12, Yanghe North Road, Yanghe Industrial Development Zone, Liuzhou City, Guangxi 545036, P. R. China

Experimental Section

Synthesis of materials:

In a typical process, 2.84 g $Ni(CH_3COO)_2 \cdot 4H_2O$ was added in 30 ml deionized water and then stirred vigorously until dissolved perfectly. Then a desired amount (0.001 g, 0.005 g, 0.01 g) of $Li(CH_3COO) \cdot 2H_2O$ was dissolved in the solution and stirred under 80 °C until the solution is dried. Finally, the Li^+ doped NiO nanoparticles in dark-grey were obtained by calcining the above mixture in air at 500 °C for about 2 h. X % Li-doped-NiO comparticles are written as x % Li-NiO in this work, where x is the molar ratio of Li set in experiments. For comparison, pristine NiO was prepared with the identical technology without adding $Li(CH_3COO) \cdot 2H_2O$.

Characterization

X−ray diffraction profiles were recorded by a RIGAKU Rint−2000 X−ray diffractometer equipped with graphite monochromatized Cu−Kα radiation (λ=1.54184 Å). Scanning electron microscopy (SEM) and electron energy loss spectroscopy (EELS) spectrum was collected on a FEI Helios Nanolab 600i field emission scanning electron microscopy. Transmission electron microscope (TEM) and High Resolution Transmission electron microscope (HRTEM) images was recorded by FEI Tecnai G2 F20 field emission transmission electron microscopy operated at 200 kV. The Raman spectroscopy spectra were recorded using LabRAM HR800. The X−ray photoelectron spectroscopy spectra were performed using a Thermo Fisher ESCALAB 250Xi spectrophotometer. All XPS spectra were calibrated by C 1s at 284.6 eV (adventitious carbon). The X-ray absorption spectroscopy experiments were

performed at the National Synchrotron Radiation Research Center (NSRRC) in Taiwan.

Three-electrodes electrochemical measurement

Electrochemical experiments were measured on a CHI 760E electrochemical workstation in a three-electrode cell and gas flow control systems at room temperature. Hg/HgO (1M KOH-filled) electrode was used as reference electrode and carbon rod electrode was acted as counter electrode. The Carbon fiber paper (CP) modified with catalyst was used as the working electrode. The catalyst ink was prepared by dispersing a 10 mg catalyst in 1 mL ethanol and 1 mL deionized water to form ethanol/water solution. Subsequently, 20 μL Nafion solution (Nafion D-521 5% w/w in water and 1-propano, Alfa Aesar Co. Ltd.) was added to the ink as a proton conducting binder to ensure good adhesion onto the CP. To form a homogeneous solution, the catalyst ink was ultrasonic dispersed for 30 min and vigorous stirred for 12 h at room temperature. After polishing the electrode with a suspension of alumina, the surface of CP (0.25 cm^2) was coated with 15 μL of the catalyst ink to make the catalyst on the working electrode was about 0.3 mg cm^{-2}. The pasted catalyst on the working electrode was dried at 60 °C in air. All OER measurements were carried out in 1 M KOH electrolyte solution which was purged with high-purity nitrogen about 15 min. All polarization curves were corrected with 95% iR compensation. Cyclic voltammograms (CVs) were performed with 100 cycles to reach the stabilization. The linear sweep voltammetry (LSV) curve was recorded with a scan rate of 10 mVs^{-1} with the Stirring speed of 1000 rpm. The current density was normalized to the

geometrical surface area and the potentials (vs. Hg/HgO) were corrected to the reversible hydrogen electrode (RHE) according to the equation: $E_{RHE} = E_{Hg/HgO} + 0.059 \times pH + 0.098$. Tafel slope was obtained from the corresponding LSV curves according to the equation: $Ŋ=a + b*\log j$ (Ŋ is overpotential, j is anodic current density, and b is Tafel slope). The electrochemical impedance spectroscopy (EIS) was measured at 1.53 V (vs. RHE) in the frequency range from 10^5 to 0.1 Hz with an amplitude of 10 mV. The cycling stability curve was collected by a chronopotentiometry response in 1 M KOH solution at the current density of 10 mA cm^{-2} for several hours.

Calculation of spin polarized DOS

Calculations were carried out using Vienna Ab initio Simulation Package (VASP). Projector augmented wave (PAW) was adopted to describe electron interactions. The Perdew-Burke-Ernzerhof (PBE) functional with a generalized gradient approximation (GGA) was used to describe the exchange-correlation interaction. To confirm the strong correlated electronic states in Ni, the GGA+U method was used, where the on-site Coulomb repulsion (Hubbard U) and the atomic orbital intraexchange (Hund's parameter J) are simplified to U_{eff} using this equation: $U_{eff} = U - J$. In this work, we choose the values of U_{eff} to be 6.3 eV for Ni. During structure optimization and DOS calculation, all energies change criterion was set to 10^{-5} eV and the bulk modle is shown in Fig. S4, the atoms were relaxed until the force acting on each atom was less than 0.02 eV $Å^{-1}$, and the plane wave cutoff was set to 450 eV. Fig. S6 show the slab models of NiO, Li-NiO, respectively. All the model construction with a 15 Å vacuum

layer region in the z direction to minimize the interactions between adjacent image cells by relaxed via the conjugate-gradient method. The k-point grids were set to be 3×3×1 for all compute instances, for lattice optimization with energy convergence and spin polarized DOS calculations.
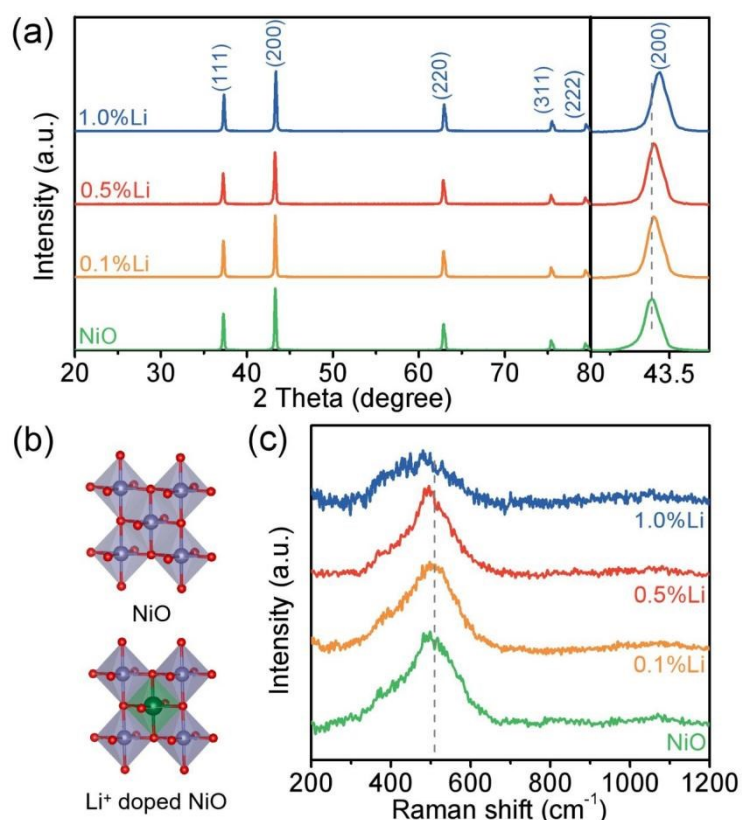
Additional Figures and Tables

Fig. S1 (a) XRD pattern, crystal structure, and Raman spectra of NiO and Li$^+$ doped NiO.

As displayed in Fig. S1a, the X-ray diffraction (XRD) patterns reveal that all as synthesized products are indexed to NiO with cubic phase structure (JCPDS No. 47-1049).[1] There is no other peaks appeared, indicating that the obtained products have high purity. The right side displays the magnified area at peak (200), exhibiting that these peaks shift slightly with the doping amount of Li$^+$ increases from 0 to 1.0 %. That is attributed to that Li$^+$ atoms occupy the site of Ni atom (Fig. S1b) and causes decreased cell lattice volume from 73.164 to 72.679 Å^3 (Table S1). To further identify the changes of crystal structure, the spectra of room temperature Raman spectroscopy are analyzed. As illustrated in Fig. S1c, the most obvious peak at 508.7 cm^{-1} refers to symmetric stretching vibration of Ni-O vibration in pure NiO.[1] A slightly shift towards lower location of the peak is observed with the increasing doping amount of Li$^+$ from

0.1 % (497.1 cm^{-1}) to 1.0 % (459.9 cm^{-1}), corresponding to stronger interactions between Ni and O. Such a change is arisen from the transmission of electrons from Ni^{2+} to Li^{+} and leads to higher electropositivity of Ni^{2+}. [1] It is worth noting that the full widths at half maximum of Raman peaks become broad with low height with the increase of Li^{+} concentration, which is due to that the stochastic distribution of Li^{+} in the NiO crystal lattice enhances the scattering of phonons.[2]
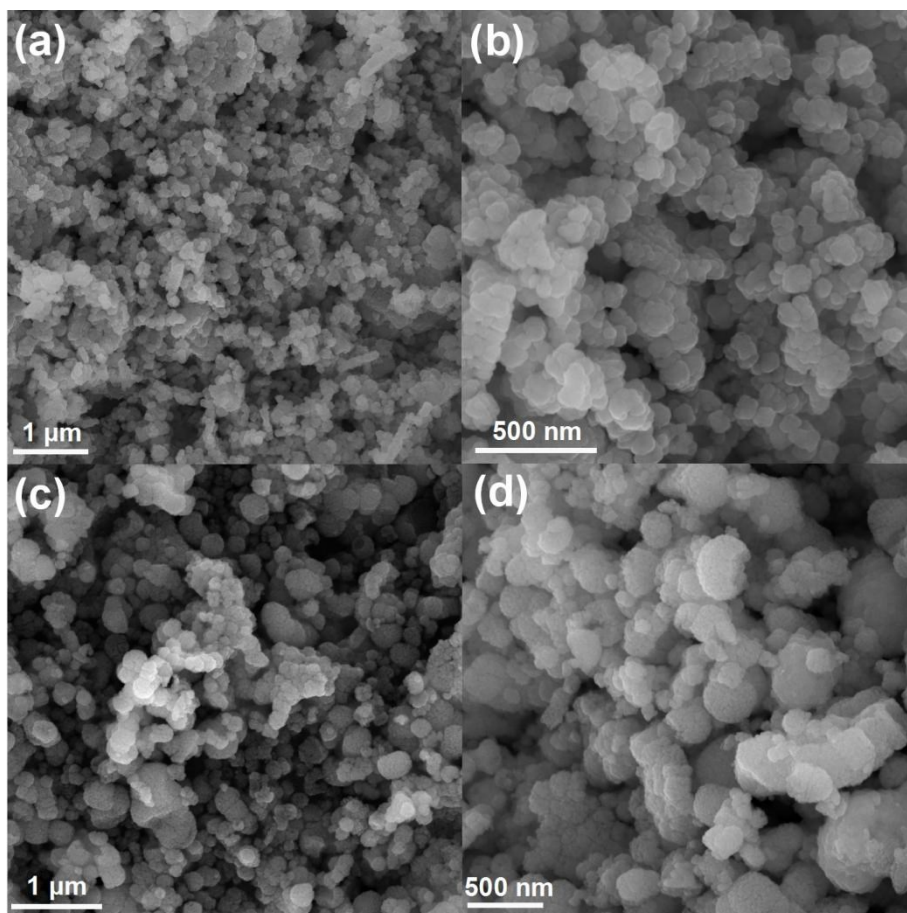
Fig. S2 (a-b) SEM images of 0.5% Li-NiO; (c-d) SEM images of pristine NiO.

The SEM images of 0.5% Li-NiO are presented in Fig. S2(a-b), and Fig. S2(c-d)

correspond to pristine NiO. As shown in the images, both 0.5% Li-NiO and pristine

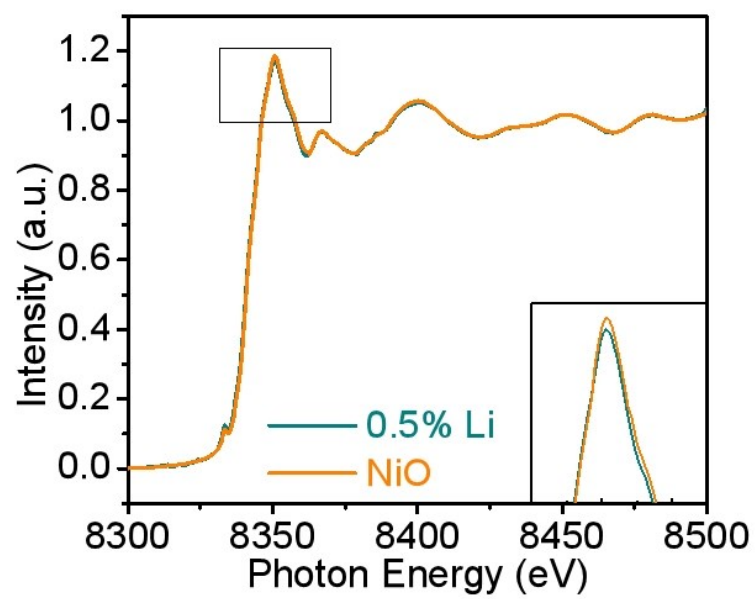NiO are particle-like and agglomerated. There is no obvious change of morphology

after Li doping.

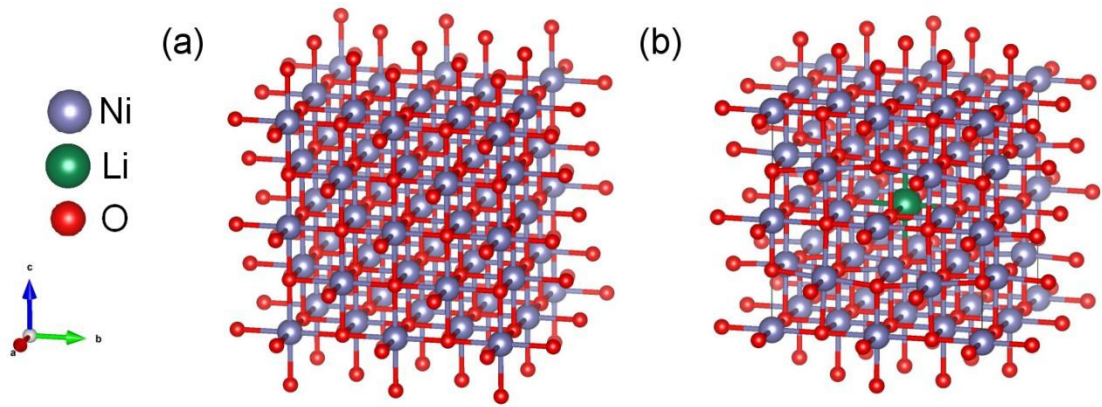Fig. S3 X-ray absorption near edge structure (XANES) of Ni K-edge.

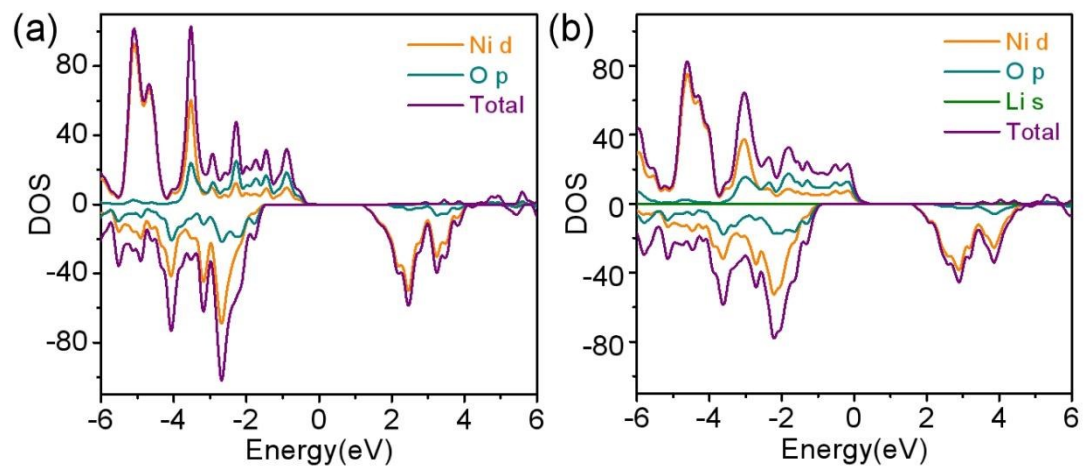Fig. S4 Model of (a) NiO and (b) Li doped NiO.

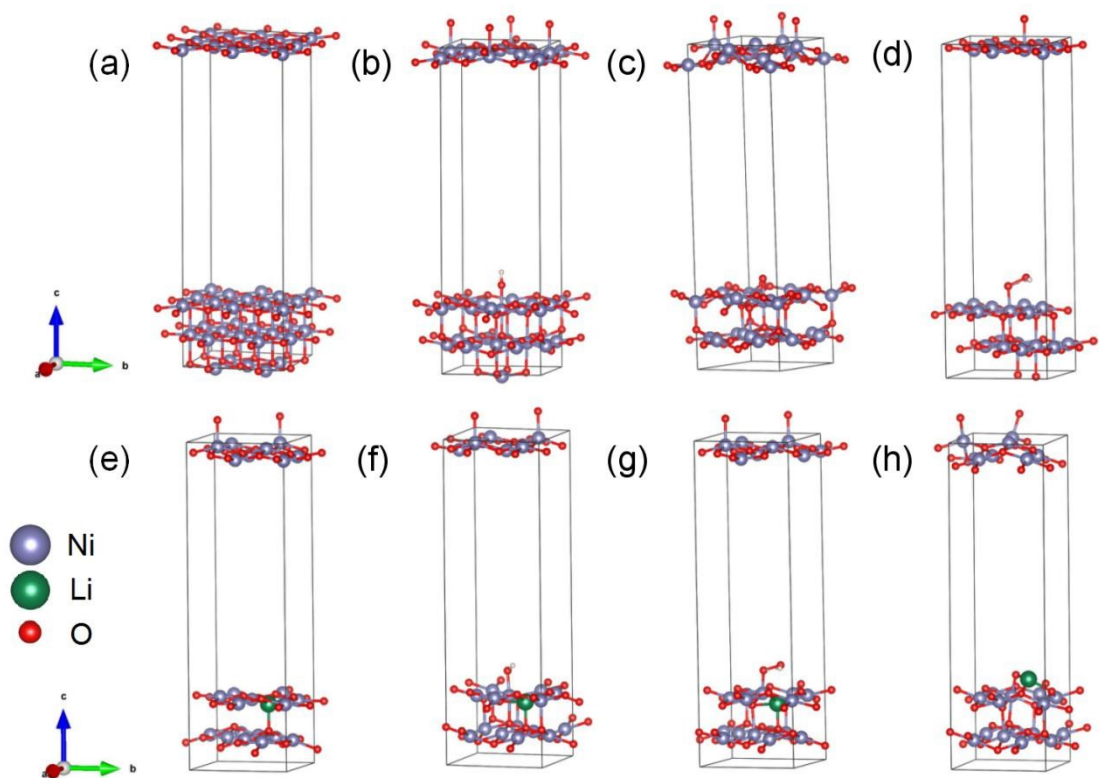Fig. S5 The density of states (DOS) of (a) NiO and (b) Li$^+$ doped NiO.

Fig. S6 The optimized atomic models for OER internediates adsorptions of (a-d) NiO
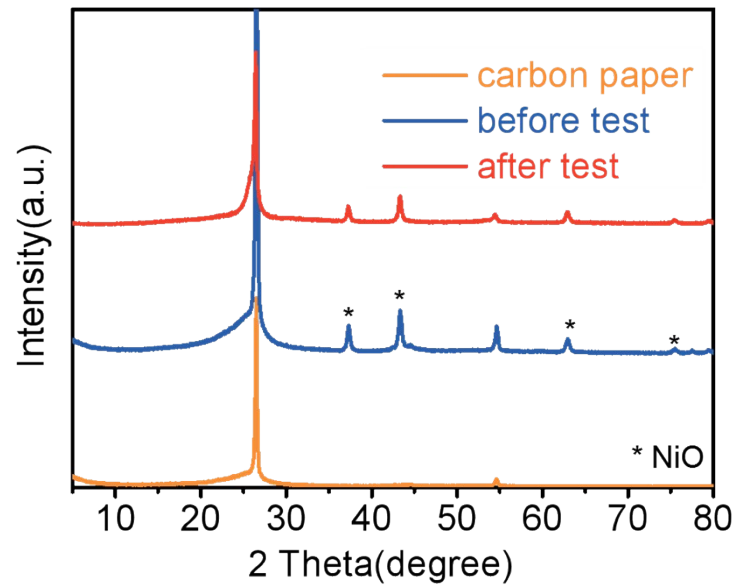
and (e-h) Li-doped-NiO

Fig. S7 The XRD pattern of 0.5% Li-NiO. The catalyst is coated on carbon paper and the electrolyte is 1M KOH, the chronopotentiometry test lasts 70 h with the current density of 10 mA cm^{-2}.
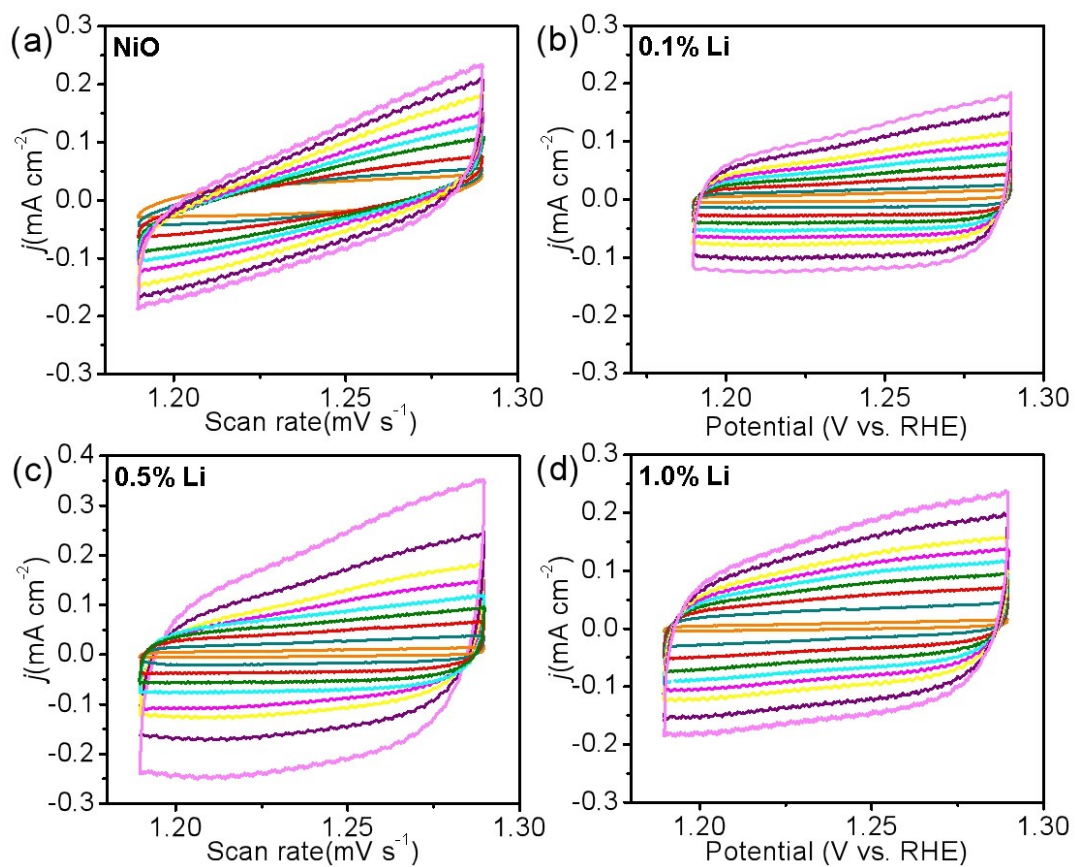
Fig. S8 The CV curves under different scanning rates at a constant voltage range from 1.19 V to 1.29 V vs. RHE: (a) NiO, (b) 0.1 % Li-NiO, (c) 0.5 % Li-NiO, and (d) 1.0 % Li-NiO.
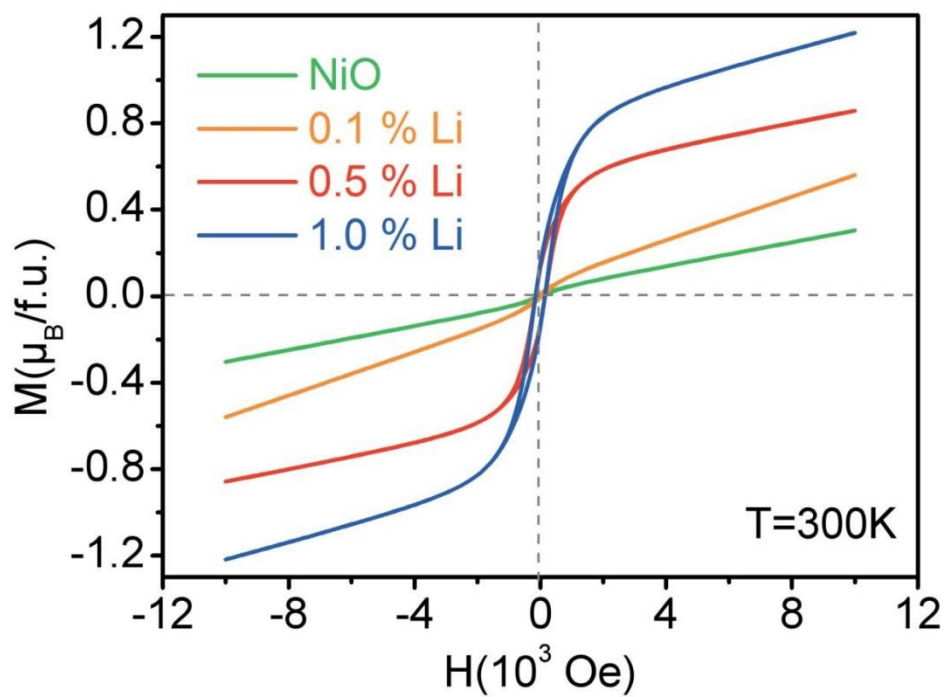
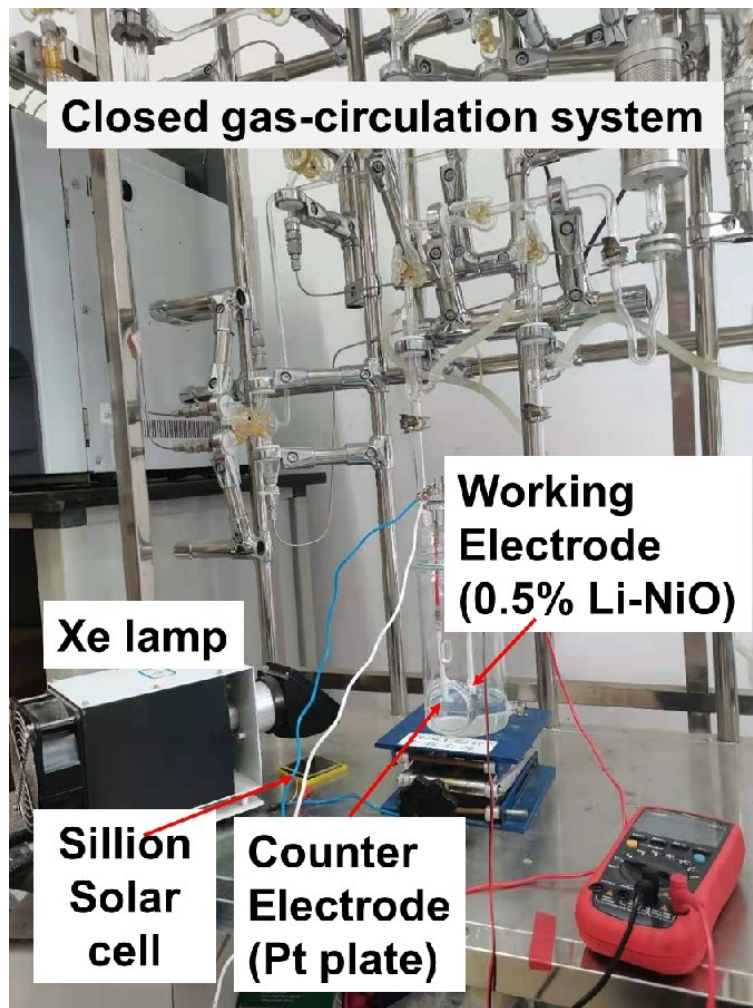Fig. S9 The magnetic hysteresis loop of Li doped NiO.

Fig. S10 The photograph of photovoltaic-electrocatalytic water splitting system.
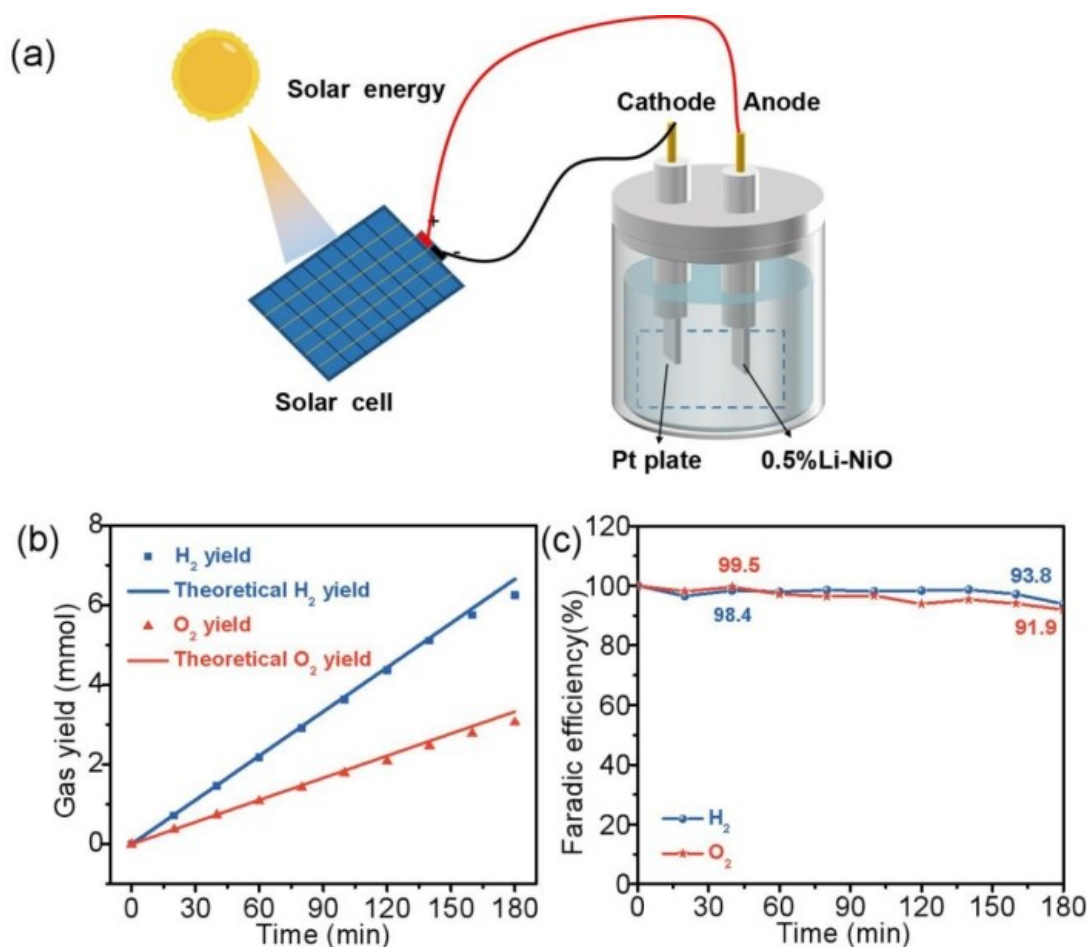
Fig. S11 (a) structure diagram of the device; (b) H_2 and O_2 yields in 1 M KOH (the blue and red lines represent the theoretical yield at 100 % Faradaic efficiency); (c)The calclulated Faradaic efficiency at the first hour.

Conversion of water into hydrogen via solar energy is a promising method to obtain clean and sustainable energy. To investigate the possible practical application of 0.5 % Li-NiO, a demonstrate system of overall water splitting is established. In this system, the electrodes connect to a crystalline silicon solar cell (Fig. S10 and Fig. S11a). The Ni foam supported 0.5 % Li-NiO and Pt plate are employed as anode and cathod respectively. A Xe lamp is used as light source with wavelength from 200 to 1000 nm (Fig. S12). To keep the voltage supplied by the crystalline silicon solar cell at 2.30 V, the intensity of Xe lamp was regulated. The practical current is 119.8 mA on the basis of the LSV curve in Fig. S13. It is shown in Fig. S11b that the producing rates of H_2

and O_2 are 2.17 and 1.11 mmol h^{-1} for the first hour, respectively. Obviously, the amount of H_2 is almost double more than that of O_2. As the production of H_2 and O_2 in theory calculated according to the experiment condition, the Faradaic efficiency for overall water splitting is 97.2 % (Fig. S11c). Based on the intensity of Xe lamp, the energy conversion yield of photo-to-H_2 is calculated as 9.52 %. Therefore, it provides an effective method to utilize solar energy to produce hydrogen energy by employing Li^+ doped NiO as electrocatalyst.
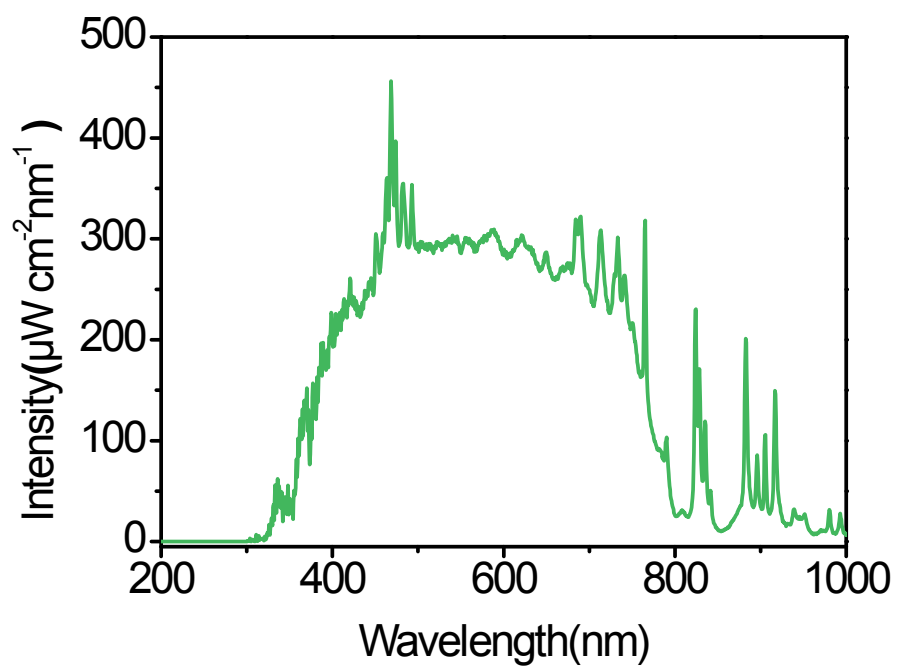
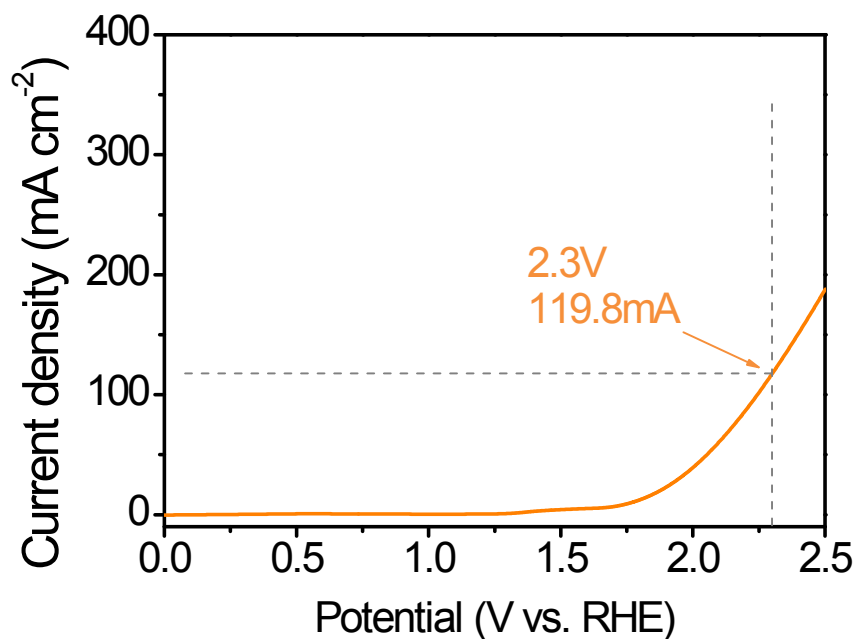Fig. S12 Irradiation spectrum of the Xe lamp.

Fig. S13 The LSV curve of 0.5 % Li-NiO with two electrode in 1 M KOH.

Calculation of Solar-to-Hydrogen Energy Conversion Efficiency

As shown in Fig. S12, the light intensity of Xe lamp is concentrated on the wavelength range of 200 - 1000 nm. The average integral light intensity measured by the light meter is 0.1258 W cm^{-2}. The irradiated area for the silicon solar cell is 14.4 cm^2. The standard molar enthalpy of combustion for H_2 is -285.84 KJ mol^{-1}. The yield of H_2 during the first hour is 2173.04 μmol. The calculation steps are as following:

Input:

Solar energy (J) = light intensity (W cm^{-2}) × illumination area (cm^2) × time (s) = 0.1258 W cm^{-2} × 14.4 cm^2 × 3600 s = 6521.472 J =6.521 kJ

Output:

H_2 energy (kJ) = standard molar enthalpy of combustion (kJ mol^{-1}) × H_2 moles (mol) = 285.84 kJ mol^{-1} × 2173.04 × 10^{-6} mol = 0.621 kJ

Solar-to-Hydrogen energy conversion efficiency = H_2 energy (kJ) / Solar energy (kJ)

= 0.621 / 6.521 = 9.52%

Calculation of the Faraday Efficiency

Faraday efficiency was defined as the ratio between the actual and theoretical amount of the product. The total charge ($Q = I \times t$) passed during the reaction was divided by $n \times F$ (n is the number of electron transfer, F is the Faraday constant) to get the theoretical gas yield. m is the actual moles of the product (2173.04 μmol during the first hour). The calculation process for the Faraday efficiency is as following:

Faraday efficiency = actual gas yield / theoretical gas yield = m / [($I \times t$) / ($n \times F$)] = ($m \times n \times F$) / ($I \times t$) = (2173.04 × 10^{-6} mol × 2 × 96485 C mol^{-1}) / (119.8 × 10^{-3} A × 3600 s) = 97.2%

Table S1. Cell lattice parameter of x % Li doped NiO (x=0,0.1,0.5,1.0)

Sample	lattice parameters	Cell volume	error
0	4.18246	73.16365	0.00818
0.1 % Li-NiO	4.18206	73.14266	0.00716
0.5 % Li-NiO	4.17851	72.95656	0.00092
1.0 % Li-NiO	4.17320	72.67877	0.00084

Table S2. Comparisons of OER performance over Ni-based catalysts in alkaline medium.

Catalyst	WE[a]	Electrolyte	j[b]	H[c]	TS[d]	Ref
Ag/NiO nanocomposites	GC	0.1M KOH	10	263	65	3
Co-doped NiO/CuO	NF	1.0M KOH	20	264	96.4	4
Ni/NiO/Fe$_3$O$_4$	GC	1.0M KOH	10	258	62	5
NiO-(La$_{0.613}$Ca$_{0.387}$)$_2$NiO$_{3.562}$ nano hybrid	GC	0.1M KOH	10	373	42	6
defect-rich NiO-MOF	NF	1.0M KOH	50	250	88.6	7
NiO nanorodss	GC	6.0M KOH	10	390	/	8
Co-NiO coreshell	GC	1.0M KOH	10	360	99	9
NiO nanowires/FTO	GC	0.1M KOH	10	363	/	10
Ni$_2$P	NF	1.0M KOH	10	400	78	11
Fe-NiO	GC	1.0M KOH	10	206	49.4	12
Ni$_{2-x}$Fe$_x$O	GC	0.5M KOH	10	325	53	13
N-NiO nanosheets	GC	1.0M KOH	10	270	83	11
Pt/NiO	GC	1.0M KOH	10	358	33	14
Ni-N-O	GC	1.0M KOH	10	300	74	15
NiO/MnO$_2$	RDE	0.1M KOH	10	390	51	16
NiO/Co$_3$O$_4$@NC	GC	1.0M KOH	10	260	73	17
LiNi$_{0.9}$Fe$_{0.1}$O$_2$	RDE	1.0M KOH	5.16	400	46.2	18
0.5% Li-NiO	CP	1.0M KOH	10	289	58.1	*

a) WE refers to working electrode (GC, Glass carbon; NF, Ni foam; RDE, Roating disk electrode; CP, Carbon fiber paper); b) j represents current density (mA cm^{-2}); c) overpotential (mV); d) TS refers to Tafel slope.

Table S3. EIS fitting data of Li doped NiO.

Products	R_s(ohm)	R_{oad}(ohm)	R_{ct}(ohm)
NiO	5.148	60.74	3.73
0.1 % Li-NiO	4.691	38.89	1.99
0.5 % Li-NiO	3.971	9.06	1.53
1.0 % Li-NiO	4.467	24.83	1.76

References

1   C. Liao, B. Yang, N. Zhang, M. Liu, G. Chen, X. Jiang, G. Chen, J. Yang, X. Liu, T. Chan, Y. Lu, R. Ma and W. Zhou, *Adv. Funct. Mater.*, 2019, **29**, 1904020.

2   K.-W. Nam and K.-B. Kim, *J. Electrochem. Soc.*, 2002, **149**, A346.

3   M. Z. Iqbal and R. J. Kriek, *Electrocatalysis*, 2018, **9**, 279–286.

4   Z. Guo, X. Wang, Y. Gao and Z. Liu, *Dalt. Trans.*, 2020, **49**, 1776–1784.

5   Y. Xie, X. Wang, K. Tang, Q. Li and C. Yan, *Electrochim. Acta*, 2018, **264**, 225–232.

6   R. Liu, F. Liang, W. Zhou, Y. Yang and Z. Zhu, *Nano Energy*, 2015, **12**, 115–122.

7   Q. Hu, X. Huang, Z. Wang, G. Li, Z. Han, H. Yang, X. Ren, Q. Zhang, J. Liu and C. He, *J. Mater. Chem. A*, 2020, **8**, 2140–2146.

8   T. Zhang, M. Y. Wu, D. Y. Yan, J. Mao, H. Liu, W. Bin Hu, X. W. Du, T. Ling and S. Z. Qiao, *Nano Energy*, 2018, **43**, 103–109.

9   Y. Ma, X. Wang, X. Sun, T. Gao, Y. Liu, L. Zhang, Q. Huo and Z. A. Qiao, *Inorg. Chem. Front.*, 2018, **5**, 1199–1206.

10   P. Manivasakan, P. Ramasamy and J. Kim, *RSC Adv.*, 2015, **5**, 33269–33274.

11   Q. Wang, Z. Liu, H. Zhao, H. Huang, H. Jiao and Y. Du, *J. Mater. Chem. A*, 2018, **6**, 18720–18727.

12   N. Zhou, N. Wang, Z. Wu and L. Li, *Catalysts*, 2018, **8**, 509.

13   A. C. Pebley, E. Decolvenaere, T. M. Pollock and M. J. Gordon, *Nanoscale*,

2017, **9**, 15070–15082.

14   C. Lin, Y. Zhao, H. Zhang, S. Xie, Y. F. Li, X. Li, Z. Jiang and Z. P. Liu, *Chem. Sci.*, 2018, **9**, 6803–6812.

15   J. Huang, Y. Sun, X. Du, Y. Zhang, C. Wu, C. Yan, Y. Yan, G. Zou, W. Wu, R. Lu, Y. Li and J. Xiong, *Adv. Mater.*, 2018, **30**, 1803367.

16   J. He, M. Wang, W. Wang, R. Miao, W. Zhong, S. Y. Chen, S. Poges, T. Jafari, W. Song, J. Liu and S. L. Suib, *ACS Appl. Mater. Interfaces*, 2017, **9**, 42676–42687.

17   M. Tahir, L. Pan, R. Zhang, Y. C. Wang, G. Shen, I. Aslam, M. A. Qadeer, N. Mahmood, W. Xu, L. Wang, X. Zhang and J. J. Zou, *ACS Energy Lett.*, 2017, **2**, 2177–2182.

18   G. Fu, X. Wen, S. Xi, Z. Chen, W. Li, J. Y. Zhang, A. Tadich, R. Wu, D. C. Qi, Y. Du, J. Cheng and K. H. L. Zhang, *Chem. Mater.*, 2019, **31**, 419–428.